J. Fluid Mech. (1994), *vol.* 268, *pp.* 267–292

Gravitational and zero-drag motion of a spheroid adjacent to an inclined plane at low Reynolds number

By RICHARD HSU† AND PETER GANATOS

Department of Mechanical Engineering, The City College of The City University of New York, New York, NY 10031, USA

(Received 28 January 1988 and in revised form 10 August 1993)

The first highly accurate solutions for the resistance tensor of an oblate or prolate spheroid moving near a planar wall obtained by Hsu & Ganatos (1989) are used to compute the translational and angular velocities and trajectories of a neutrally buoyant spheroid in shear flow and the gravitational settling motion of a non-neutrally buoyant spheroid adjacent to an inclined plane. The neutrally buoyant spheroid in shear flow undergoes a periodical motion toward and away from the wall as it continually tumbles forward. For some orientation angles it is found that the wall actually enhances the angular velocity of the particle. For certain inclinations a spheroid settling under gravity near an inclined plane reaches an equilibrium position, after which it translates parallel to the wall without rotation.

1. Introduction

The creeping motion of a non-spherical particle in a viscous fluid adjacent to a planar boundary has been a problem of long standing interest. Some biological and engineering applications of the theory include modelling the flow of red blood cells in the microcirculation, study of the diffusive and convective transport of non-spherical macromolecules or solute particles in intercellular clefts or through porous membranes, and determination of the trajectory of a contaminant particle in a lubricating bearing or in the laminar sublayer in the vicinity of a turbine blade.

This classic low-Reynolds-number flow problem has previously been studied by a number of investigators using various techniques. A far-field solution for the motion of a spheroid at an arbitrary angle of attack adjacent to a planar wall was obtained by Wakiya (1959) using the method of reflections. More recently, using the method of distributing internal singularities, Yang & Leal (1983, 1984) studied the motion of a slender body near a flat fluid–fluid interface (the interface behaves like a rigid wall in the limit as the viscosity of the fluid not containing the body becomes large) and Dabros (1985) obtained the angular velocity of a neutrally buoyant prolate spheroid in shear flow adjacent to a planar wall.

Most recently, the boundary integral technique was used by Hsu & Ganatos (1989) to obtain solutions for the resistance tensor for any arbitrary body of revolution tumbling adjacent to a planar wall at low Reynolds number. The force and torque were accurately computed for an oblate or prolate spheroid, a torus and a biconcave shaped disk translating parallel or perpendicular to the wall, rotating about an axis parallel to the wall, or rigidly held in place in a shear flow. The key features of these solutions are

† Current address: Department of Physiology, University of Arizona, Tucson, Arizona 85724, USA.

that the no-slip boundary conditions are satisfied exactly along the planar boundary by using Blake's (1971) solution for the flow induced by a point force (stokeslet) adjacent to a planar boundary as the kernel function in the integral formulation, a double Fourier–Legendre series is used to describe the unknown stress distribution on the particle surface and the unknown coefficients contained in this series are determined by satisfying the no-slip boundary conditions at discrete points on the particle surface using a boundary collocation technique. The accuracy of the solutions has been tested by comparison with the exact bipolar coordinate solutions of Brenner (1961) for the motion of a sphere perpendicular to the wall and Goldman, Cox & Brenner (1967*a*, *b*) for a sphere translating parallel to a wall, rotating adjacent to a wall or rigidly held in place in shear flow. The solutions obtained by the boundary integral method were found to be in very good agreement with the exact solutions down to a gap width of a tenth of a sphere radius. On the other hand, it was found that the solutions of Wakiya (1959) obtained by the method of reflections are accurate only when the spheroid–wall distance is at least five times the semi-major axis of the spheriod.

For the motion of a sphere near a planar wall, some of the elements of the resistance tensor are identically zero, such as the coefficients which give the force perpendicular to the wall arising from translatory motion of the particle parallel to the wall or rotation about an axis parallel to the wall. However, in general, these forces are not zero for a spheroid. The hydrodynamic force and torque on a spheroid depend strongly on its orientation relative to the wall. This characteristic feature complicates the motion of a spheroid adjacent to a plane.

In this paper we consider only motion where the axis of symmetry of the body lies in a plane perpendicular to the plane of the wall and the fluid motion is symmetric about this plane. Jeffery (1922) has shown that for unbounded flow in the zero Reynolds number limit, this type of motion is neutrally stable for both oblate and prolate spheroids. This may also be expected to be the case in the presence of the wall. Thus both oblate and prolate spheroids are considered in the present study.

In Hsu & Ganatos (1989) it was shown that the force and torque experienced by an oblate spheroid having an aspect ratio $\epsilon = 0.5$ in the vicinity of a planar wall was remarkably similar to the force and torque experienced by a torus or a biconcave shaped disk having the same aspect ratio. We would therefore expect that many of the predictions for the motion of an oblate spheroid to be presented in the present paper are equally applicable for a torus or a biconcave shaped disk, at least qualitatively.

In the present work, strong-interaction solutions are presented for the zero-drag and gravitational motion of a spheroid adjacent to an inclined planar boundary. The zero-drag motions are of interest in various applications where dispersed small particles are carried along by the fluid such as red blood cells in the microcirculation or contaminant particles in a lubricating bearing. The gravitational motion solutions are of interest in studies of sedimentation and resuspension phenomena. The paper is presented in four sections. Section 2 contains the formulation relating the force and torque acting on the particle in quasi-steady motion near a planar wall to the fluid and particle velocities. In §3, solutions are presented for the zero-drag motion of a spheroid in shear flow next to a planar wall. Section 4 contains solutions for the velocities and trajectories of a spheroid settling under gravity next to an inclined plane. Finally, §5 contains some concluding remarks on applicability of the solution procedure to some closely related problems.

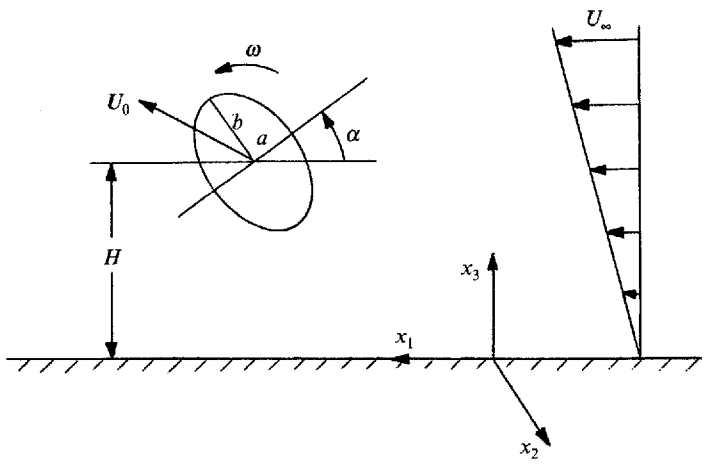

FIGURE 1. Geometry of planar motion of a spheroid adjacent to a wall.

2. General motion of a spheroid adjacent to a planar wall

Consider the motion of a spheroid adjacent to a planar wall as shown in figure 1. The spheroid has a half-length a and radius b. It is spaced at a distance H from the wall and has an orientation angle α relative to the wall. The spheroid is translating in the (x_1, x_3)-plane with velocity U_0 which has components U_1 and U_3, and rotating about the x_2-axis with angular velocity ω. A shear flow $U_\infty = Sx_3$ may be present in the x_1-direction.

In the zero Reynolds number limit the fluid velocity V must satisfy the creeping flow equations

$$\mu\nabla^2 V = \nabla p, \quad \nabla\cdot V = 0, \tag{2.1a,b}$$

subject to the boundary conditions

$$V = \omega\times\rho + U_0 \quad \text{at the particle surface,} \tag{2.2a}$$

$$V = 0 \quad \text{at the wall,} \tag{2.2b}$$

$$V = U_\infty, \quad p = 0 \quad \text{at infinity,} \tag{2.2c}$$

where ρ is the position vector whose origin is at the particle centre.

It was shown in Hsu & Ganatos (1989) that the force and torque acting on a spheroid whose axis of symmetry lies in a plane perpendicular to the wall in planar symmetric flow may be expressed using twelve resistance coefficients as follows:

$$\begin{bmatrix} F_1 \\ F_3 \\ T_2 \end{bmatrix} = 6\pi\mu c \begin{bmatrix} F_1^{t_1} & F_1^{t_3} & F_1^{r} & HF_1^{s} \\ F_3^{t_1} & F_3^{t_3} & F_3^{r} & HF_3^{s} \\ \frac{4}{3}bT_2^{t_1} & \frac{4}{3}bT_2^{t_3} & \frac{4}{3}bT_2^{r} & \frac{2}{3}b^2T_2^{s} \end{bmatrix} \begin{bmatrix} U_1 \\ U_3 \\ b\omega \\ S \end{bmatrix}. \tag{2.3}$$

Here F_1 and F_3 are the force components in the x_1- and x_3-directions, respectively, T_2 is the torque on the spheroid and c is the semi-major axis given by $c = b$ for an oblate spheroid and $c = a$ for a prolate spheroid. The twelve resistance coefficients depend on the aspect ratio ϵ defined as a/b for an oblate spheroid and b/a for a prolate spheroid (such that $0 < \epsilon < 1$ in both cases), the separation distance H/c and the orientation

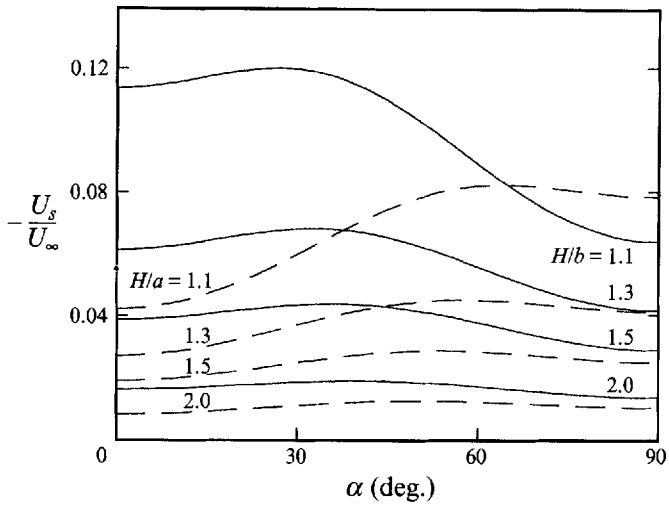

FIGURE 2. The slip velocity of a neutrally buoyant spheroid with $\epsilon = 0.5$ in shear flow; ——, oblate spheroid; – – –, prolate spheroid.

angle relative to the wall α. Of the twelve resistance coefficients three pairs are related according to the reciprocity relations (Brenner 1964):

$$F_1^{t_3} = F_3^{t_1}, \quad F_1^r = \tfrac{4}{3}T_2^{t_1}, \quad F_3^r = \tfrac{4}{3}T_2^{t_3}. \tag{2.4a–c}$$

The nine independent force and torque coefficients have been computed to a high degree of accuracy using the boundary integral method by Hsu & Ganatos (1989). Therefore if the force and torque on the spheroid are prescribed, the system of linear equations (2.3) may be solved for the unknown velocity components U_1, U_3 and ω. We now consider two special cases, the zero-drag motion of a spheroid adjacent to a wall and the gravitational settling motion of a spheroid in the vicinity of an inclined plane.

3. Zero-drag motion of a spheroid in shear flow

In this section we consider the motion of a neutrally buoyant spheroid in shear flow adjacent to a planar wall. From (2.3) the conditions of zero drag and zero torque require

$$F_1^{t_1} U_1 + F_1^{t_3} U_3 + bF_1^{r_\omega} + HF_1^s S = 0, \tag{3.1a}$$

$$F_3^{t_1} U_1 + F_3^{t_3} U_3 + bF_3^{r_\omega} \omega + HF_3^s S = 0, \tag{3.1b}$$

$$T_2^{t_1} U_1 + T_2^{t_3} U_3 + bT_2^{r_2} + \tfrac{1}{2}bT_2^s S = 0. \tag{3.1c}$$

Simultaneous solution of these three linear equations gives the three velocity components of the spheroid U_1, U_3 and ω. Solutions for an oblate or prolate spheroid having aspect ratio $\epsilon = 0.5$ are presented as functions of particle orientation α and particle-to-wall spacing H/c in figures 2–4. The velocity component U_1 and angular velocity ω are even functions of α, while the velocity component U_3 is an odd function of α. As expected from symmetry, all velocity components have a periodicity of 180° Therefore they are plotted only in the range between 0° and 90°.

For the velocity component U_1, the quantity of greatest interest is the local slip velocity U_s of the spheroid centre relative to the incoming fluid velocity U_∞ defined by

$$U_s = U_1 - U_\infty = U_1 - HS. \tag{3.2}$$

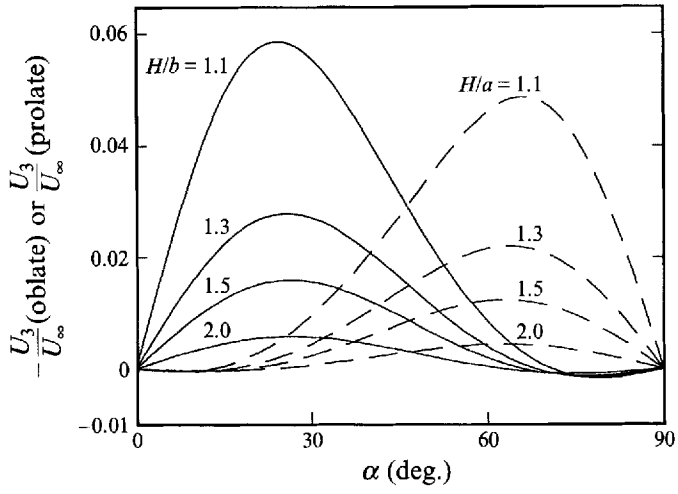

FIGURE 3. The velocity component perpendicular to the wall of a neutrally buoyant spheroid with $\epsilon = 0.5$ in shear flow; ——, oblate spheroid; – – –, prolate spheroid.

Figure 2 shows the slip velocity as a function of α at constant H/c for an oblate or prolate spheroid with $\epsilon = 0.5$. The slip velocity is negative for all orientation angles and separation distances, indicating that an oblate or prolate spheroid always lags the fluid in shear flow. For a given separation distance the oblate spheroid experiences minimum slip at an orientation angle $\alpha = 90°$ while the prolate spheroid experiences minimum slip at $\alpha = 0°$. Maximum slip for the oblate spheroid occurs at an orientation of roughly 30° while for the prolate spheroid it occurs at approximately 60°.

Figure 3 shows the variation of the perpendicular velocity component U_3 with orientation angle for the same conditions as in figure 2. Here a positive U_3 indicates that the spheroid is moving away from the wall. For small positive orientation angles of an oblate spheroid and close particle–wall spacings, the major axis of the spheroid is nearly touching the wall. This end of the spheroid experiences a large resistance to motion as can be seen from the large slip velocity in figure 2. The incoming flow strikes the spheroid nearly head-on causing it to pivot about the point closest to the wall in a counterclockwise direction. This results in a motion of the centre of the spheroid toward the wall as seen by the large negative value of U_3 shown in figure 3 near $\alpha = 25°$. For a prolate spheroid this phenomenon may be seen in figure 3 for orientation angles which are large. In this case the spheroid pivots about its tip in a counterclockwise direction resulting in a motion of the centre of the spheroid away from the wall as evidenced by the large value of U_3 near $\alpha = 65°$ in figure 3. Another peculiar feature which may be seen in figure 3 is that U_3 changes sign and vanishes not only for α equal to 0° and 90° as expected from symmetry but also at a particular angle in between. This occurs when the velocity component perpendicular to the wall induced by the translatory motion of the spheroid parallel to the wall exactly balances the velocity component perpendicular to the wall induced by the rotational motion of the spheroid.

The angular velocity ω is shown in figure 4. The angular velocity is always positive indicating that with the shear flow directed along the x_1-axis as shown in figure 1, the spheroid tumbles about the x_3-axis in a counterclockwise direction. For an oblate spheroid, the angular velocity is maximum at $\alpha = 0°$ and monotonically decreases to its minimum value at $\alpha = 90°$. For a prolate spheroid, the angular velocity is minimum

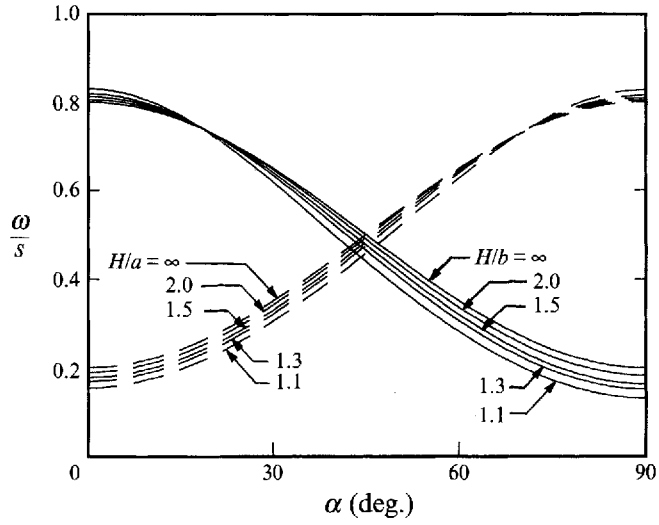

FIGURE 4. The angular velocity of a neutrally buoyant spheroid with $\epsilon = 0.5$ in shear flow; ——, oblate spheroid; – – –, prolate spheroid.

at $\alpha = 0°$ and increases to its maximum at $\alpha = 90°$. The maximum angular velocity occurs when the semi-major axis of the spheroid lies perpendicular to the incoming shear flow since in this orientation the incoming flow exerts the largest torque on the particle. Also plotted is the angular velocity of an isolated spheroid ($H/c = \infty$) which is given by (3.5). Over most of the range of α the wall acts to reduce the angular velocity of the particle. However, when the major axis of the particle is oriented within roughly 20° of the axis perpendicular to the wall, the wall actually enhances the angular velocity of the particle. This occurs because the translational motion of the particle parallel to the wall causes the particle to roll along the wall and this contribution to the angular velocity is in addition to the angular velocity induced by the shear flow in the absence of the wall. Unlike the velocity components U_1 and U_3, which are strong functions of separation distance, the angular velocity ω changes very little with separation distance in the range $1.1 \leqslant H/c < \infty$ especially when α is close to 20° for an oblate spheroid and 70° for a prolate spheroid.

Examination of figures 2–4 shows that the variation of the translational and rotational velocity components of a prolate spheroid with orientation angle α is qualitatively similar to that of an oblate spheroid having the same aspect ratio at an orientation of $90° - \alpha$. This is because while the angle between the major axis and the wall is α for a prolate spheroid, it is $90° - \alpha$ for an oblate spheroid.

We next consider the trajectory of the particle in shear flow. The equations of motion of the particle in dimensionless form are:

$$\frac{\mathrm{d}x_1^*}{\mathrm{d}t^*} = \frac{U_1}{U_\infty}\frac{H}{c}, \quad \frac{\mathrm{d}x_3^*}{\mathrm{d}t^*} = \frac{U_3}{U_\infty}\frac{H}{c}, \quad \frac{\mathrm{d}\alpha}{\mathrm{d}t^*} = \frac{\omega}{S}, \tag{3.3a–c}$$

where $x_1^* = x_1/c, x_3^* = x_3/c$ and $t^* = tS$.

To compute the three velocity components in equations (3.1) for a single separation distance and orientation angle using the boundary integral method requires approximately 1–10 minutes CPU time on an IBM 3081 computer, depending on particle–wall distance. Therefore it is impractical that all velocities needed to solve the differential equations (3.3) at each instant of time be computed by the boundary

(*a*) Oblate spheroid

	$\epsilon = 0.1$				$\epsilon = 0.5$			
H/c	a_0	a_2	a_4	a_6	a_0	a_2	a_4	a_6
1.1	0.0307	0.0069	−0.0205	−0.0037	0.0991	0.0269	−0.0105	−0.0020
1.3	0.0192	0.0034	−0.0128	−0.0013	0.0584	0.0106	−0.0069	−0.0008
1.5	0.0125	0.0016	−0.0083	−0.0009	0.0382	0.0052	−0.0045	−0.0003
1.75	0.0080	0.0007	−0.0057	−0.0001	0.0244	0.0025	−0.0029	0
2.0	0.0055	0.0004	−0.0037	0	0.0166	0.0013	−0.0020	0
2.5	0.0029	0.0002	−0.0019	0	0.0087	0.0005	−0.0010	0
∞	0	0	0	0	0	0	0	0

(*b*) Prolate spheroid

	$\epsilon = 0.1$				$\epsilon = 0.5$			
H/c	a_0	a_2	a_4	a_6	a_0	a_2	a_4	a_6
1.1	0.0086	−0.0019	−0.0065	0.0010	0.0673	−0.0195	−0.0071	0.0014
1.3	0.0051	−0.0006	−0.0039	0.0007	0.0386	−0.0074	−0.0045	0.0004
1.5	0.0034	−0.0002	−0.0025	0.0003	0.0249	−0.0032	−0.0031	0.0002
1.75	0.0021	−0.0002	−0.0018	0.0002	0.0158	−0.0017	−0.0023	0.0002
2.0	0.0013	0	−0.0011	0	0.0106	−0.0011	−0.0015	0
2.5	0.0005	0	−0.0006	0	0.0055	0	−0.0006	0
∞	0	0	0	0	0	0	0	0

TABLE 1. The coefficients of $-U_s/U_\infty$ in (3.4*a*)

integral method. Instead, we utilize interpolating functions in the form of a truncated Fourier series:

$$-\frac{U_s}{U_\infty} = a_0 + a_2\cos 2\alpha + a_4\cos 4\alpha + a_6\cos 6\alpha, \tag{3.4a}$$

$$-\frac{U_3}{U_\infty} = b_2\sin 2\alpha + b_4\sin 4\alpha + b_6\sin 6\alpha + b_8\sin 8\alpha, \tag{3.4b}$$

$$\frac{\omega}{S} = c_0 + c_2\cos 2\alpha + c_4\cos 4\alpha + c_6\cos 6\alpha, \tag{3.4c}$$

where a_n, b_n and c_n are unknown functions of the aspect ratio ϵ and the particle–wall spacing H/c. For a given H/c the velocity components are computed by the boundary integral method at seven orientation angles and the coefficients a_n, b_n and c_n are calculated using a least squares fit. Tables 1–3 list values of these coefficients for an oblate or prolate spheroid with aspect ratios $\epsilon = 0.1$ and 0.5 at selected values of H/c. Intermediate values of the difference between the coefficients at arbitrary H/c and $H/c \to \infty$ are obtained by interpolation using cubic splines on a log–log scale. This difference is then added to the value at $H/c \to \infty$ to obtain the value of the coefficient at any arbitrary H/c. By comparison with the values obtained directly by solving equations (3.1) the velocities calculated by equations (3.4) have an error of less than 4% for both oblate and prolate spheroids. At $H/c = \infty$ the coefficients $a_n, b_n = 0$ for all $n \geqslant 0$, $c_0 = \frac{1}{2}$, $c_2 = (b^2 - a^2)/[2(b^2 + a^2)]$ and $c_n = 0$ for $n > 2$. The differential equations (3.3) were solved numerically using a fourth-order Runge–Kutta procedure.

Figure 5 shows the trajectories of the centre of a tumbling neutrally buoyant oblate or prolate spheroid in shear flow for two aspect ratios, $\epsilon = 0.1$ and 0.5. In all cases the spheroid begins its quasi-steady motion at the point $x_1^* = 0$, $x_3^* = 1.25$ with initial

(*a*) Oblate spheroid

	$\epsilon = 0.1$				$\epsilon = 0.5$			
H/c	b_2	b_4	b_6	b_8	b_2	b_4	b_6	b_8
1.1	0.02654	0.03424	0.00544	0.00117	0.03692	0.02821	0.00553	0.00102
1.3	0.01341	0.01967	0.00195	0.00023	0.01790	0.01356	0.00154	0.00018
1.5	0.00844	0.01282	0.00089	0	0.01007	0.00792	0.00057	0.00005
1.75	0.00488	0.00814	0.00038	0	0.00559	0.00468	0.00021	0.00001
2.0	0.00310	0.00557	0.00022	0	0.00348	0.00309	0.00010	0
2.5	0.00128	0.00310	0.00008	0	0.00161	0.00157	0.00003	0
∞	0	0	0	0	0	0	0	0

(*b*) Prolate spheroid

	$\epsilon = 0.1$				$\epsilon = 0.5$			
H/c	b_2	b_4	b_6	b_8	b_2	b_4	b_6	b_8
1.1	−0.01345	0.01316	−0.00249	0.00061	−0.03209	0.02233	−0.00480	0.00123
1.3	−0.00674	0.00689	−0.00077	0.00011	−0.01496	0.01004	−0.00118	0.00017
1.5	−0.00392	0.00422	−0.00032	0.00003	−0.00833	0.00571	−0.00043	0.00006
1.75	−0.00226	0.00259	−0.00014	0.00001	−0.00463	0.00334	−0.00017	0.00002
2.0	−0.00143	0.00171	−0.00007	0	−0.00284	0.00216	−0.00008	0
2.5	−0.00068	0.00087	−0.00002	0	−0.00130	0.00107	−0.00002	0
∞	0	0	0	0	0	0	0	0

TABLE 2. The coefficients of $-U_3/U_\infty$ in (3.4*b*)

(*a*) Oblate spheroid

	$\epsilon = 0.1$				$\epsilon = 0.5$			
H/c	c_0	c_2	c_4	c_6	c_0	c_2	c_4	c_6
1.1	0.4847	0.4974	0.0170	0.0042	0.4600	0.3453	0.0212	0.0041
1.3	0.4897	0.4951	0.0100	0.0019	0.4746	0.3316	0.0109	0.0018
1.5	0.4928	0.4936	0.0061	0.0007	0.4822	0.3232	0.0057	0.0013
1.75	0.4953	0.4928	0.0042	0.0006	0.4885	0.3155	0.0036	0.0006
2.0	0.4967	0.4920	0.0029	0.0003	0.4921	0.3112	0.0026	0.0001
2.5	0.4982	0.4912	0.0015	0.0002	0.4956	0.3060	0.0011	0.0001
∞	0.5	0.4901	0	0	0.5	0.3	0	0

(*b*) Prolate spheroid

	$\epsilon = 0.1$				$\epsilon = 0.5$			
H/c	c_0	c_2	c_4	c_6	c_0	c_2	c_4	c_6
1.1	0.4938	−0.4905	0.0063	−0.0019	0.4744	−0.3322	0.0163	−0.0042
1.3	0.4964	−0.4908	0.0037	−0.0009	0.4837	−0.3216	0.0081	−0.0013
1.5	0.4974	−0.4908	0.0026	−0.0002	0.4888	−0.3153	0.0047	−0.0002
1.75	0.4986	−0.4906	0.0015	−0.0001	0.4926	−0.3104	0.0029	−0.0001
2.0	0.4987	−0.4903	0.0010	−0.0001	0.4951	−0.3073	0.0016	−0.0001
2.5	0.4993	−0.4902	0.0005	0	0.4972	−0.3041	0.0008	0
∞	0.5	−0.4901	0	0	0.5	−0.3	0	0

TABLE 3. The coefficients of ω/S in (3.4*c*)

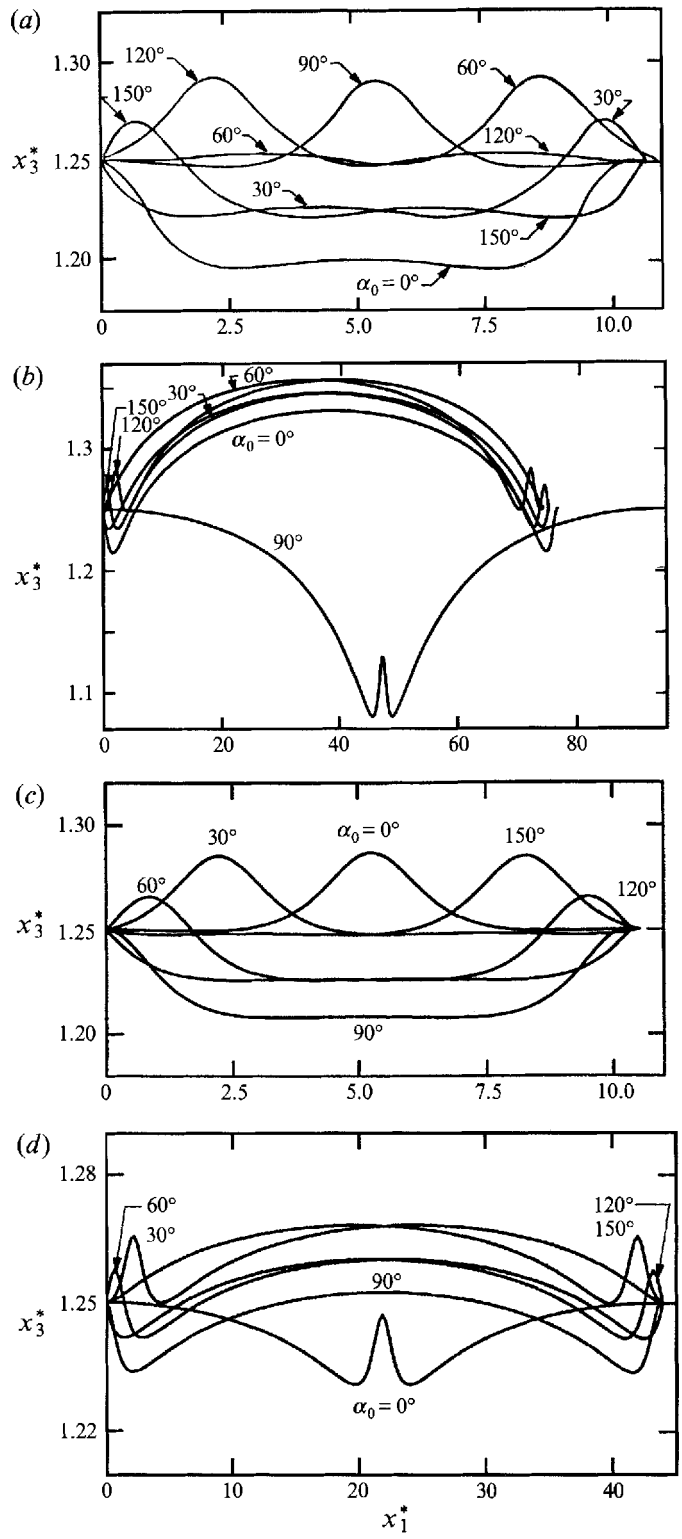

FIGURE 5. Trajectories of the centre of a neutrally buoyant spheroid in shear flow (*a*) oblate, $\epsilon = 0.5$; (*b*) oblate, $\epsilon = 0.1$; (*c*) prolate, $\epsilon = 0.5$; (*d*) prolate, $\epsilon = 0.1$. Coordinates non-dimensionalized by length of semi-major axis *c*.

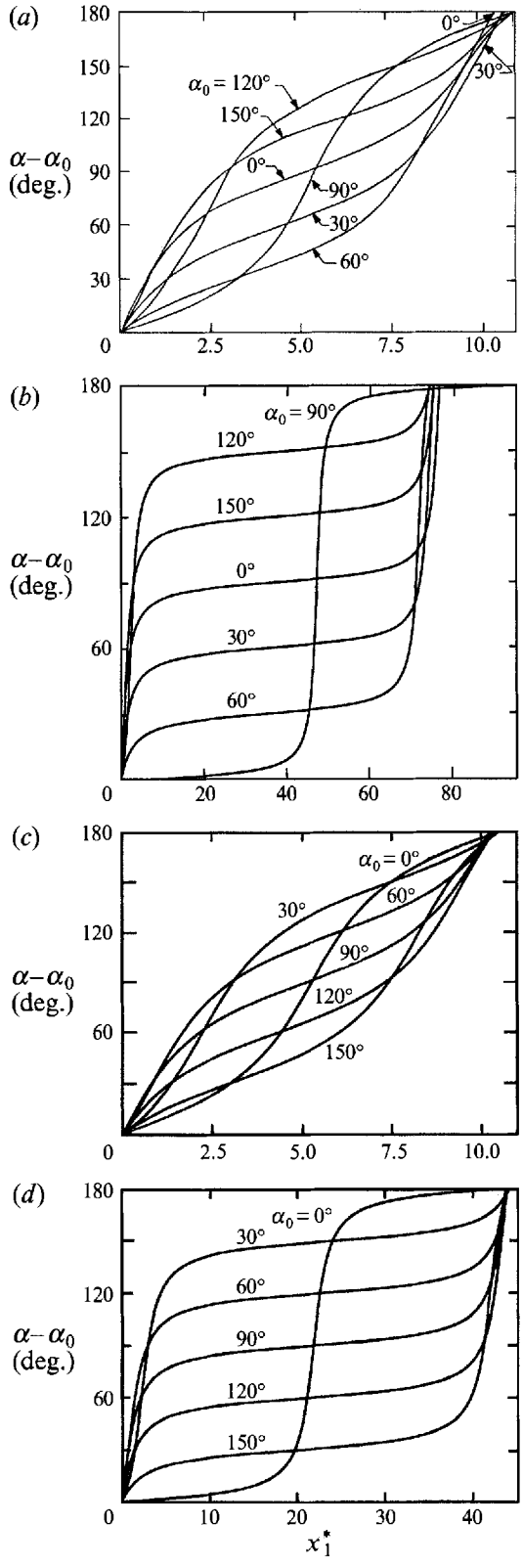

FIGURE 6. Variation of the orientation angle of a neutrally buoyant spheroid in shear flow (*a*) oblate, $\epsilon = 0.5$; (*b*) oblate, $\epsilon = 0.1$; (*c*) prolate, $\epsilon = 0.5$; (*d*) prolate, $\epsilon = 0.1$.

orientation angle α_0. For clarity the scale in the x_3^*-direction has been greatly expanded. One notes that the wall has a strong influence on the trajectory of the particle. The spheroid centre does not move in a straight line as it would in unbounded flow. Although the velocity component perpendicular to the wall is zero when the spheroid axis is parallel or perpendicular to the wall, these positions cannot be maintained owing to the rotation. Therefore when the particle is translating parallel to the plane, it also drifts toward and away from the plane periodically. The lobes appearing in the curves are the result of the spheroid pivoting about its tip when it is in close proximity to the wall as explained earlier. For small aspect ratios the pivoting action is sharper and the lobes appear as spikes in figures 5(*b*) and 5(*d*). Figure 6 gives the corresponding orientation angle for the trajectories shown in figure 5. The angular velocity ω is never zero as shown in figure 4, so the particle continually rotates in one direction. The sharp changes in orientation angle α seen in figure 6 (especially evident in figures 6(*b*) and 6(*d*) for $\epsilon = 0.1$) are also the result of the spheroid pivoting about its end. The trajectory of the particle centre and the period of the motion strongly depend on the body's aspect ratio, its initial orientation angle as well as its initial distance from the boundary.

For a neutrally buoyant oblate or prolate spheroid in unbounded shear flow, the orientation angle satisfies the differential equation, Jeffery (1922):

$$\frac{\mathrm{d}\alpha}{\mathrm{d}t^*} = \frac{1}{2}\left[1 + \frac{b^2 - a^2}{b^2 + a^2}\cos 2\alpha\right]. \tag{3.5}$$

The solution of (3.5) is

$$\alpha = \tan^{-1}\left[\frac{b}{a}\tan\frac{ab}{b^2 + a^2}t^*\right]. \tag{3.6}$$

Therefore the dimensionless period of a spheroid in unbounded shear flow is $T_\infty^* = T_\infty S = 2\pi(a^2 + b^2)/(ab)$. Figure 7 shows the variation of the rotational period T of an oblate or prolate spheroid with $\epsilon = 0.1$ and 0.5 as a function of the initial separation distance x_3^* and orientation angle α_0. The period is minimum when the particle is far from the wall and increases continuously (without limit) as the initial particle–wall spacing is decreased. For an oblate spheroid with $\epsilon = 0.1$ at a given initial distance from the wall, the period increases with increasing initial orientation from 0° to 90°. For $\epsilon = 0.5$ the period decreases with increasing initial orientation angle. As expected the period becomes independent of α_0 with increasing distance from the wall. For a prolate spheroid with $\epsilon = 0.5$ the period increases with increasing initial orientation angle. The variation of the period of a prolate spheroid having $\epsilon = 0.1$ with initial orientation angle is too small to be seen on the scale of figure 7.

4. Spheroid settling under gravity adjacent to an inclined plane

We now consider the motion of a spheroid settling under gravity adjacent to a plane wall which is inclined at an angle β with quiescent fluid at infinity as shown in figure 8. Using (2.3), a force and torque balance on the particle yields

$$6\pi\mu c[F_1^{t_1} U_1 + F_1^{t_3} U_3 + bF_1^r \omega] + \tfrac{4}{3}\pi ab^2(\rho_s - \rho) g \sin\beta = 0, \tag{4.1a}$$

$$6\pi\mu c[F_3^{t_1} U_1 + F_3^{t_3} U_3 + bF_3^r \omega] - \tfrac{4}{3}\pi ab^2(\rho_s - \rho) g \cos\beta = 0, \tag{4.1b}$$

$$T_2^{t_1} U_1 + T_2^{t_3} U_3 + bT_2^r \omega = 0, \tag{4.1c}$$

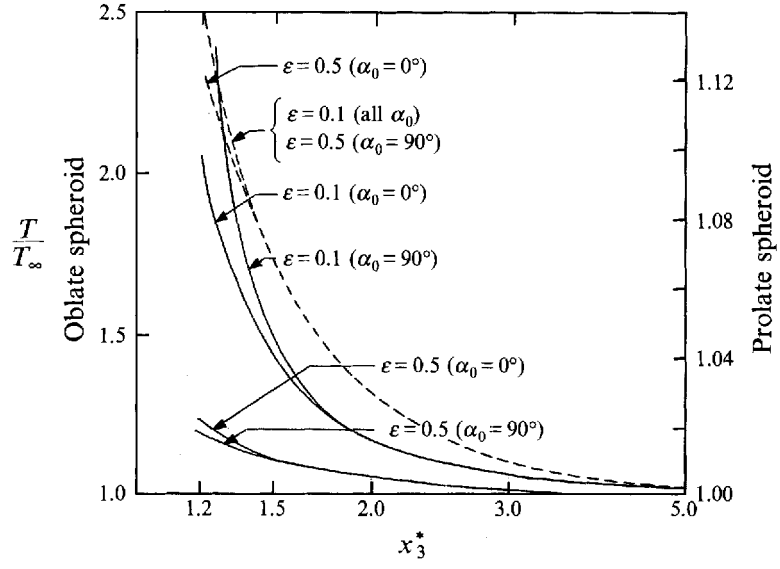

FIGURE 7. Variation of the period T of a spheroid with initial separation distance x_3^* and orientation angle α_0; ——, oblate spheroid; – – –, prolate spheroid.

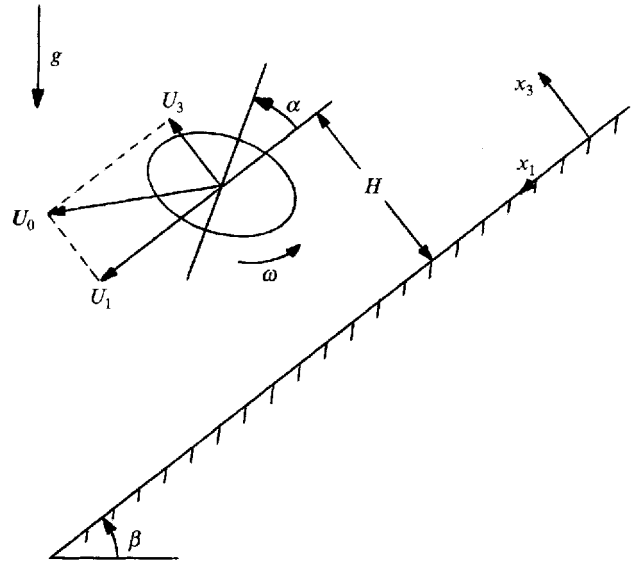

FIGURE 8. Schematic diagram of a spheroid settling under gravity adjacent to a plane.

where ρ_s and ρ are the density of the particle and the fluid, respectively, and g is the acceleration due to gravity. These three equations may be solved simultaneously to yield the two translational components U_1 and U_3 and angular velocity ω of the particle. In the Stokes flow limit, the settling of a spheroid adjacent to a wall inclined at an arbitrary angle β may be completely described by a linear superposition of the solutions at $\beta = 0°$ and 90°. Thus we need only consider these two special cases.

The velocity components of the particle for $\beta = 0°$, in which the plane is perpendicular to the direction of gravity, will be expressed as U_1^3, U_3^3 and ω^3. The

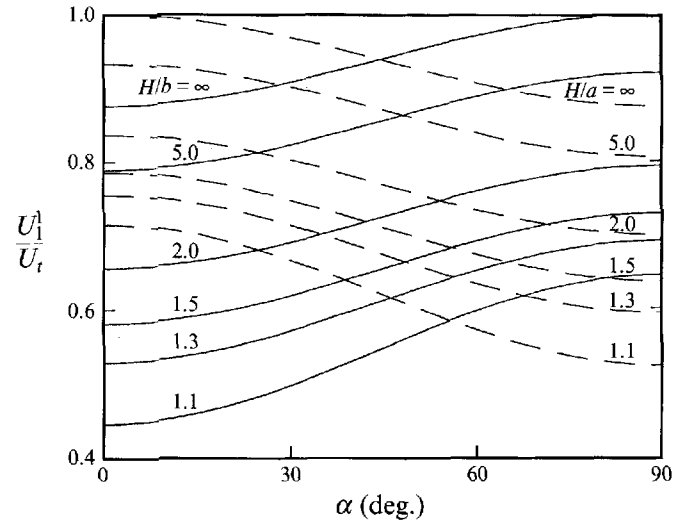

FIGURE 9. The velocity parallel to the wall of a spheroid with $\epsilon = 0.5$ settling under a gravitational force acting in the same direction; ——, oblate spheroid; – – –, prolate spheroid.

velocity components for $\beta = 90°$, where the plane is parallel to the direction of gravity, will be expressed as U_1^1, U_3^1 and ω^1. The velocity $U_1^3 = -U_3^1$ by the reciprocity relations (2.4).

The translational velocity components U_1^1, U_3^3 and U_3^1 for a spheroid settling under gravity having aspect ratio $\epsilon = 0.5$ are shown in figures 9–11, respectively, as a function of orientation angle α and particle–wall spacing H/c. All three velocities are non-dimensionalized by the terminal velocity U_t of an isolated spheroid in an unbounded fluid with the force of gravity acting parallel to its major axis. With this choice of U_t the magnitude of the dimensionless velocities is always less than unity. The terminal velocity of an oblate spheroid settling with its axis of symmetry perpendicular to the direction of gravity is given by (Happel & Brenner 1967, p. 222)

$$U_t = \frac{ab}{12}\frac{(\rho_s - \rho)g}{\mu}\left[\frac{3-2\epsilon^2}{(1-\epsilon^2)^{\frac{3}{2}}}\sin^{-1}[\sqrt{1-\epsilon^2}] - \frac{\epsilon}{1-\epsilon^2}\right], \tag{4.2a}$$

where $\epsilon = a/b$. The terminal velocity of a prolate spheroid settling with its axis of symmetry parallel to the direction of gravity is given by

$$U_t = \frac{ab}{12}\frac{(\rho_s - \rho)g}{\mu}\left[\frac{(2-\epsilon^2)\epsilon}{(1-\epsilon^2)^{\frac{3}{2}}}\ln\left[\frac{1+\sqrt{1-\epsilon^2}}{1-\sqrt{1-\epsilon^2}}\right] - \frac{2\epsilon}{1-\epsilon^2}\right], \tag{4.2b}$$

where $\epsilon = b/a$. Also plotted in figures 9–11 are the limiting values of the various velocity components for an isolated spheroid (labelled $H/c = \infty$) which may be obtained analytically. For an oblate spheroid

$$\frac{U_1^1}{U_t} = 1 - 2F(\epsilon)\cos^2\alpha, \quad -\frac{U_3^3}{U_t} = 1 - 2F(\epsilon)\sin^2\alpha, \quad \frac{U_3^1}{U_t} = F(\epsilon)\sin 2\alpha, \tag{4.3a–c}$$

while for a prolate spheroid

$$\frac{U_1^1}{U_t} = 1 - 2G(\epsilon)\sin^2\alpha, \quad -\frac{U_3^3}{U_t} = 1 - 2G(\epsilon)\cos^2\alpha, \quad -\frac{U_3^1}{U_t} = G(\epsilon)\sin 2\alpha, \tag{4.4a–c}$$

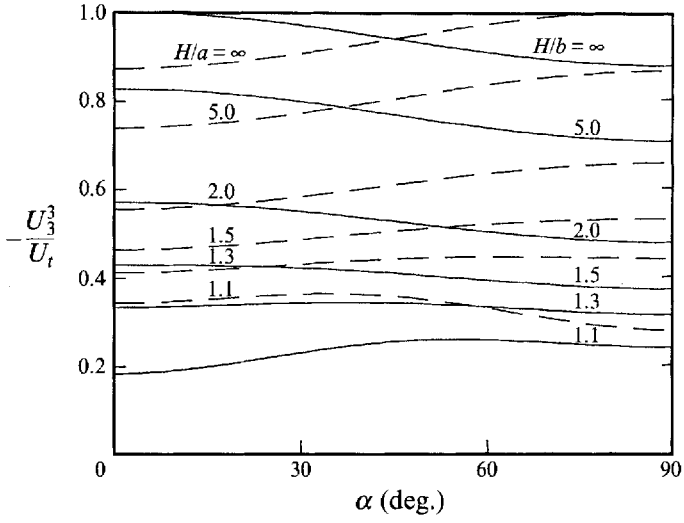

FIGURE 10. The velocity perpendicular to the wall of a spheroid with $\epsilon = 0.5$ settling under a gravitational force acting in the same direction; ——, oblate spheroid; – – –, prolate spheroid.

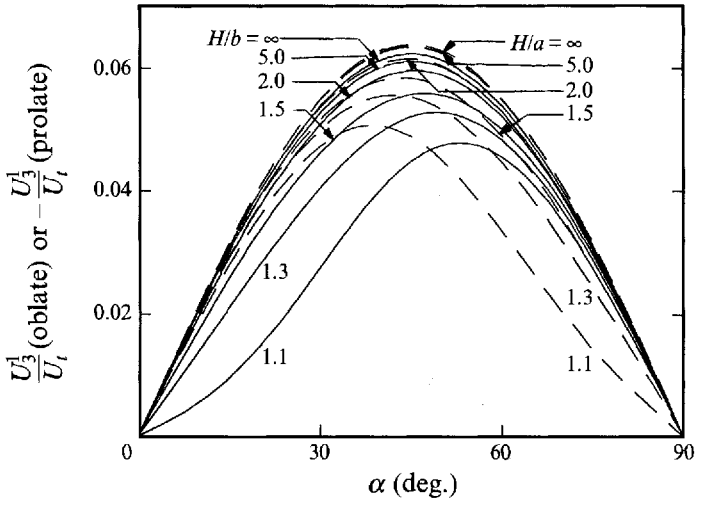

FIGURE 11. The velocity perpendicular to the wall of a spheroid with $\epsilon = 0.5$ settling under a gravitational force acting parallel to the wall; ——, oblate spheroid; – – –, prolate spheroid.

where

$$F(\epsilon) = \frac{1}{2} - \frac{\epsilon\sqrt{1-\epsilon^2} + (1-2\epsilon^2)\sin^{-1}\sqrt{1-\epsilon^2}}{-\epsilon\sqrt{1-\epsilon^2} - (2\epsilon^2-3)\sin^{-1}\sqrt{1-\epsilon^2}}, \tag{4.5a}$$

and

$$G(\epsilon) = \frac{1}{2} - \frac{\sqrt{1-\epsilon^2} + (2-3\epsilon^2)\ln\dfrac{1+\sqrt{1-\epsilon^2}}{\epsilon}}{-4\sqrt{1-\epsilon^2} + 2(2-\epsilon^2)\ln\dfrac{1+\sqrt{1-\epsilon^2}}{1-\sqrt{1-\epsilon^2}}}. \tag{4.5b}$$

The angular velocities ω^1 and ω^3 are non-dimensionalized by U_t/c and plotted in figures 12 and 13. Both ω^1 and ω^3 vanish as $H/c \to \infty$. The translational velocities U_1^1, U_3^3 and

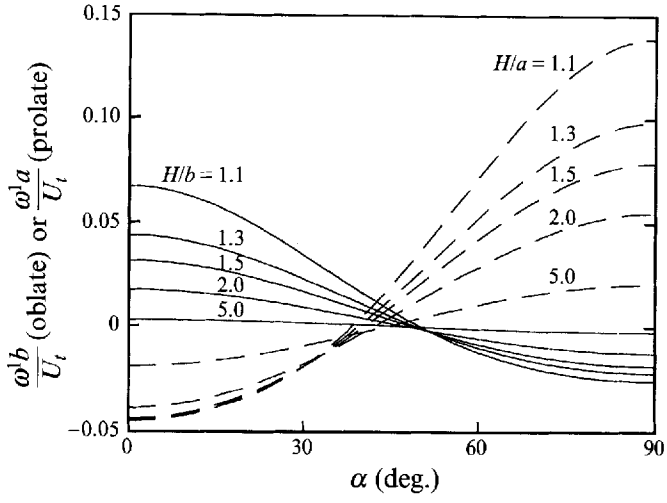

FIGURE 12. The angular velocity of a spheroid with $\epsilon = 0.5$ settling under a gravitational force acting parallel to the wall; ——, oblate spheroid; – – –, prolate spheroid.

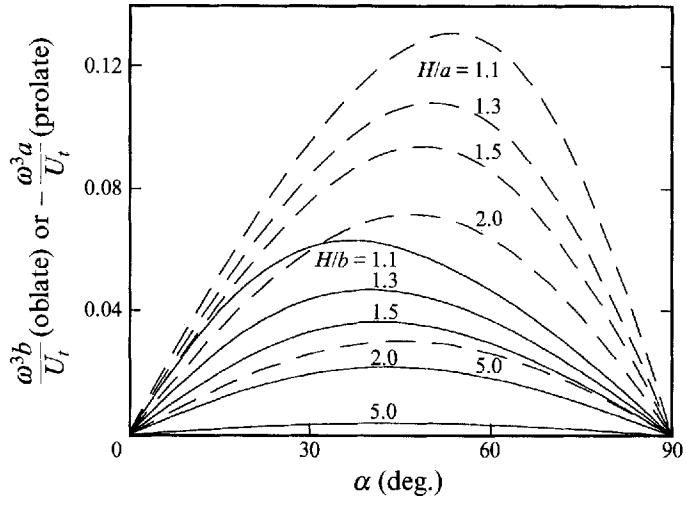

FIGURE 13. The angular velocity of a spheroid with $\epsilon = 0.5$ settling under a gravitational force acting perpendicular to the wall; ——, oblate spheroid; – – –, prolate spheroid.

rotational velocity ω^1 are even functions of α while U_3^1 and ω^3 are odd functions of α. Thus they are plotted only in the range between 0° and 90°. In this range of α, U_1^1 is always positive and U_3^3 is always negative indicating that their direction corresponds to the direction of the gravitational force. U_1^1 is maximum at the orientation angle for which the cross-sectional area of the spheroid normal to x_1 is minimum and decreases with decreasing distance from the wall. The same is true for the magnitude of U_3^3 except at close particle–wall spacings where the wall offers a great deal of resistance to motion when the semi-major axis of the particle is oriented nearly perpendicular to the wall. For $0 < \alpha < 90°$, U_3^1 is always positive for an oblate spheroid indicating that with the gravitational force acting in the x_1-direction, the particle drifts away from the wall. In the same range of α, U_3^1 is always negative for a prolate spheroid indicating that it moves toward the wall. The magnitude of U_3^1 decreases with decreasing particle–wall

distance as the wall interaction becomes stronger. U_3^1 changes very little with particle–wall spacing when the particle is oriented with its major axis nearly parallel to the wall.

In figures 12 and 13, a positive angular velocity indicates counterclockwise rotation as shown in figure 8. In figure 12 the wall is oriented at $\beta = 90°$ so that the force of gravity acts in the x_1-direction. When the major axis of the particle is oriented perpendicular to the wall, the angular velocity is positive indicating that the particle rolls along the wall as it settles. However, when the major axis is oriented parallel to the wall, the particle rotates in a clockwise direction as it settles. The clockwise rotation is the result of the couple induced by the pressure force in the gap between the particle and the wall which builds up on the leading half of the spheroid and is reduced on the trailing half. The angular velocity vanishes at the critical orientation of the particle where the two effects exactly balance. The angular velocity of the particle when the wall is oriented at $\beta = 0°$ with the gravitational force acting in the negative x_3-direction is shown in figure 13. For $0 < \alpha < 90°$, an oblate spheroid rotates in a counterclockwise direction while a prolate spheroid rotates in a clockwise direction as it settles. This occurs because for an oblate spheroid, the centre of the spheroid where the gravitational force acts lies to the left of the point on the surface of the particle closest to the wall, while for a prolate spheroid the centre lies to the right. As explained in the previous section, the translational and angular velocity components of a prolate spheroid at an orientation angle α vary qualitatively with α as the corresponding velocity components of an oblate spheroid at an orientation angle of $90° - \alpha$.

We next consider the trajectory of a spheroidal particle settling under gravity adjacent to an inclined planar wall. The required values of the translational and rotational velocities at an arbitrary separation distance and orientation are interpolated in the same manner as in §3 for the motion of a neutrally buoyant particle in shear flow. For an oblate or prolate spheroid the translational and rotational velocity components are approximated by the truncated Fourier series:

$$\frac{U_1^1}{U_t} = A_0 + A_2 \cos 2\alpha, \tag{4.6a}$$

$$-\frac{U_3^3}{U_t} = B_0 + B_2 \cos 2\alpha + B_4 \cos 4\alpha, \tag{4.6b}$$

$$-\frac{U_3^1}{U_t} = C_2 \sin 2\alpha + C_4 \sin 4\alpha + C_6 \sin 6\alpha, \tag{4.6c}$$

$$\frac{\omega^1 c}{U_t} = D_0 + D_2 \cos 2\alpha + D_4 \cos 4\alpha, \tag{4.6d}$$

$$\frac{\omega^3 c}{U_t} = E_2 \sin 2\alpha + E_4 \sin 4\alpha + E_6 \sin 6\alpha, \tag{4.6e}$$

where A_n, B_n, C_n, D_n and E_n are functions of aspect ratio ϵ and particle–wall spacing H/c. As $H/c \to \infty$, comparison with (4.3) and (4.4) shows that $A_n, B_n, C_n = 0$ for $n > 2$ and $D_n, E_n = 0$ for $n \geqslant 0$. For an oblate spheroid

$$A_0 = B_0 = 1 - F(\epsilon), \quad -A_2 = B_2 = -C_2 = F(\epsilon), \tag{4.7a–b}$$

while for a prolate spheroid

$$A_0 = B_0 = 1 - G(\epsilon), \quad A_2 = -B_2 = C_2 = G(\epsilon), \tag{4.8a–b}$$

	(*a*) Oblate spheroid				(*b*) Prolate spheroid			
	$\epsilon = 0.1$		$\epsilon = 0.5$		$\epsilon = 0.1$		$\epsilon = 0.5$	
H/c	A_0	A_2	A_0	A_2	A_0	A_2	A_0	A_2
1.1	0.5678	−0.1674	0.5466	−0.0998	0.7093	0.1699	0.6194	0.0967
1.3	0.6105	−0.1549	0.6111	−0.0823	0.7324	0.1622	0.6748	0.0809
1.5	0.6415	−0.1516	0.6554	−0.0747	0.7483	0.1589	0.7117	0.0743
1.75	0.6710	−0.1477	0.6954	−0.0703	0.7626	0.1565	0.7442	0.0702
2.0	0.6930	−0.1453	0.7254	−0.0679	0.7734	0.1554	0.7687	0.0678
5.0	0.7912	−0.1403	0.8541	−0.0649	0.8176	0.1530	0.8690	0.0638
∞	0.8597	−0.1403	0.9378	−0.0622	0.8473	0.1527	0.9366	0.0634

TABLE 4. The coefficients of U_1^1/U_t in (4.6*a*)

where $F(\epsilon)$ and $G(\epsilon)$ are given by (4.5). The coefficients appearing in (4.6) are tabulated for selected values of H/c and ϵ in tables 4–8 for both oblate and prolate spheroids.

The equations of motion of a particle settling under gravity adjacent to a planar wall inclined at an angle β (see figure 8) in dimensionless form are

$$\frac{dx_1^*}{dt^*} = \frac{U_1^1}{U_t}\sin\beta + \frac{U_1^3}{U_t}\cos\beta, \tag{4.9a}$$

$$\frac{dx_3^*}{dt^*} = \frac{U_3^1}{U_t}\sin\beta + \frac{U_3^3}{U_t}\cos\beta, \tag{4.9b}$$

$$\frac{d\alpha}{dt^*} = \frac{\omega^1 c}{U_t}\sin\beta + \frac{\omega^3 c}{U_t}\cos\beta, \tag{4.9c}$$

where $x_1^* = x_1/c$, $x_3^* = x_3/c$ and $t^* = U_t t/c$. The system of differential equations was solved numerically using a fourth-order Runge–Kutta procedure.

Figure 14 shows the trajectories of a spheroid falling adjacent to an inclined planar wall. Solutions are presented for an initial particle-to-wall spacing $x_3^* = 6$ and various values of initial orientation angle α_0. The initial values of x_1^* were chosen arbitrarily. For the sake of clarity the scale in the x_3^*-direction is greatly magnified. Figure 14(*a*) shows the trajectories of an oblate spheroidal particle of aspect ratio $\epsilon = 0.5$ settling adjacent to a planar wall inclined at $\beta = 85°$. A curious feature is that the spheroid eventually reaches the same equilibrium position from the wall regardless of the starting position. For some initial orientations the particle moves monotonically toward the equilibrium position while for others the particle moves toward and then away from the wall until it reaches the final position. A similar behaviour is also evident for a prolate spheroid having the same aspect ratio and wall inclination angle and for an oblate spheroid with aspect ratio $\epsilon = 0.1$ and wall inclination $\beta = 75°$. In the interest of saving space, these figures are not presented here but may be obtained from the authors upon request. For small inclination angles, the spheroid monotonically approaches the wall as shown in figure 14(*b*) for an oblate spheroid having an aspect ratio $\epsilon = 0.1$ settling next to a wall inclined at $\beta = 30°$. For this case, it is possible that an equilibrium position may still exist very close to the wall for $x_3^* < 1.1$ where it is computationally prohibitive to obtain solutions using the present theory. For large wall inclination angles, no equilibrium position exists as is evident in figure 14(*c*).

To give a full picture of the motion, the same trajectories described in figure 14 are plotted in terms of the separation distance and the orientation angle relative to the wall

(*a*) Oblate spheroid

	$\epsilon = 0.1$			$\epsilon = 0.5$		
H/c	B_0	B_2	B_4	B_0	B_2	B_4
1.1	0.330	0.061	−0.022	0.234	−0.028	−0.021
1.3	0.397	0.093	−0.010	0.333	0.010	−0.009
1.5	0.448	0.108	−0.006	0.405	0.029	−0.004
1.75	0.498	0.119	−0.003	0.472	0.041	−0.002
2.0	0.537	0.125	−0.002	0.525	0.047	−0.001
5.0	0.721	0.138	0	0.767	0.061	0
∞	0.860	0.140	0	0.938	0.062	0

(*b*) Prolate spheroid

	$\epsilon = 0.1$			$\epsilon = 0.5$		
H/c	B_0	B_2	B_4	B_0	B_2	B_4
1.1	0.577	−0.103	−0.012	0.334	0.032	−0.023
1.3	0.622	−0.126	−0.004	0.434	−0.015	−0.007
1.5	0.653	−0.136	−0.002	0.500	−0.033	−0.004
1.75	0.680	−0.142	−0.001	0.561	−0.045	−0.002
2.0	0.701	−0.146	0	0.607	−0.051	−0.001
5.0	0.788	−0.152	0	0.802	−0.063	0
∞	0.847	−0.153	0	0.937	−0.063	0

TABLE 5. The coefficients of $-U_3^3/U_t$ in (4.6*b*)

(*a*) Oblate spheroid

	$\epsilon = 0.1$			$\epsilon = 0.5$		
H/c	C_2	C_4	C_6	C_2	C_4	C_6
1.1	−0.122	0.011	0.003	−0.0422	0.0104	0.0026
1.3	−0.130	0.006	0.001	−0.0513	0.0045	0.0007
1.5	−0.133	0.003	0	−0.0556	0.0022	0
1.75	−0.136	0.002	0	−0.0581	0.0012	0
2.0	−0.137	0.001	0	−0.0595	0.0007	0
5.0	−0.140	0	0	−0.0610	0.0001	0
∞	−0.140	0	0	−0.0622	0.0	0

(*b*) Prolate spheroid

	$\epsilon = 0.1$			$\epsilon = 0.5$		
H/c	C_2	C_4	C_6	C_2	C_4	C_6
1.1	0.145	0.003	−0.0011	0.0467	0.0079	−0.0021
1.3	0.149	0.002	−0.0004	0.0547	0.0031	−0.0005
1.5	0.150	0.001	0	0.0581	0.0015	−0.0002
1.75	0.151	0	0	0.0603	0.0008	−0.0001
2.0	0.153	0	0	0.0614	0.0004	0
5.0	0.153	0	0	0.0633	0	0
∞	0.153	0	0	0.0634	0	0

TABLE 6. The coefficients of $-U_3^1/U_t$ in (4.6*c*)

(*a*) Oblate spheroid

	$\epsilon = 0.1$			$\epsilon = 0.5$		
H/c	D_0	D_2	D_4	D_0	D_2	D_4
1.1	0.0332	0.1189	0.0174	0.0140	0.0465	0.0064
1.3	0.0222	0.1024	0.0103	0.0076	0.0328	0.0029
1.5	0.0157	0.0919	0.0070	0.0046	0.0250	0.0015
1.75	0.0108	0.0819	0.0048	0.0027	0.0189	0.0009
2.0	0.0077	0.0739	0.0034	0.0017	0.0148	0.0005
5.0	0.0006	0.0330	0.0003	0	0.0026	0
∞	0	0	0	0	0	0

(*b*) Prolate spheroid

	$\epsilon = 0.1$			$\epsilon = 0.5$		
H/c	D_0	D_2	D_4	D_0	D_2	D_4
1.1	0.0223	−0.0674	0.0111	0.0329	−0.0916	0.0139
1.3	0.0131	−0.0531	0.0056	0.0195	−0.0719	0.0067
1.5	0.0087	−0.0455	0.0036	0.0131	−0.0617	0.0040
1.75	0.0057	−0.0391	0.0023	0.0086	−0.0532	0.0025
2.0	0.0039	−0.0345	0.0015	0.0059	−0.0471	0.0017
5.0	0.0003	−0.0144	0.0001	0.0003	−0.0200	0.0001
∞	0	0	0	0	0	0

TABLE 7. The coefficients of $\omega^1 c/U_t$ in (4.6*d*)

(*a*) Oblate spheroid

	$\epsilon = 0.1$			$\epsilon = 0.5$		
H/c	E_2	E_4	E_6	E_2	E_4	E_6
1.1	0.149	0.017	0.003	0.0623	0.0082	0.0015
1.3	0.139	0.012	0.001	0.0466	0.0039	0.0004
1.5	0.129	0.009	0.001	0.0361	0.0020	0
1.75	0.118	0.006	0.001	0.0277	0.0011	0
2.0	0.108	0.004	0	0.0218	0.0007	0
5.0	0.0492	0.0003	0	0.0039	0	0
∞	0	0	0	0	0	0

(*b*) Prolate spheroid

	$\epsilon = 0.1$			$\epsilon = 0.5$		
H/c	E_2	E_4	E_6	E_2	E_4	E_6
1.1	−0.0911	0.0132	−0.0026	−0.1284	0.0184	−0.0038
1.3	−0.0774	0.0075	−0.0009	−0.1072	0.0095	−0.0012
1.5	−0.0679	0.0049	−0.0004	−0.0934	0.0058	−0.0005
1.75	−0.0590	0.0031	−0.0002	−0.0809	0.0036	−0.0002
2.0	−0.0522	0.0021	−0.0001	−0.0716	0.0024	−0.0001
5.0	−0.0217	0.0001	0	−0.0301	0.0002	0
∞	0	0	0	0	0	0

TABLE 8. The coefficients of $\omega^3 c/U_t$ in (4.6*e*)

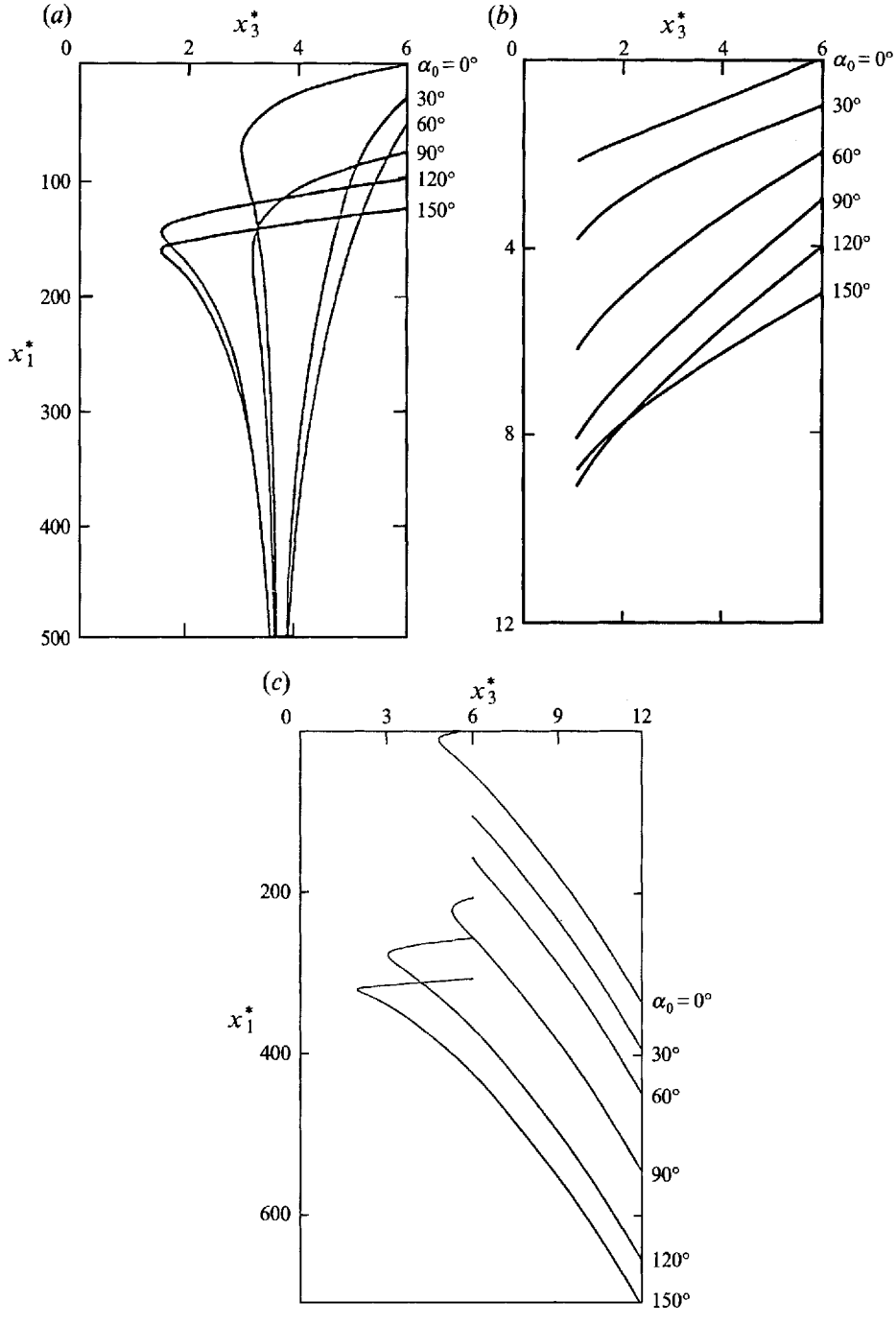

FIGURE 14. Trajectories traced by the centre of an oblate spheroid settling under gravity adjacent to an inclined plane from the initial position $x_3^* = 6$. (*a*) $\epsilon = 0.5$, $\beta = 85°$; (*b*) $\epsilon = 0.1$, $\beta = 30°$; (*c*) $\epsilon = 0.1$, $\beta = 81°$. Coordinates non-dimensionalized by length of semi-major axis c.

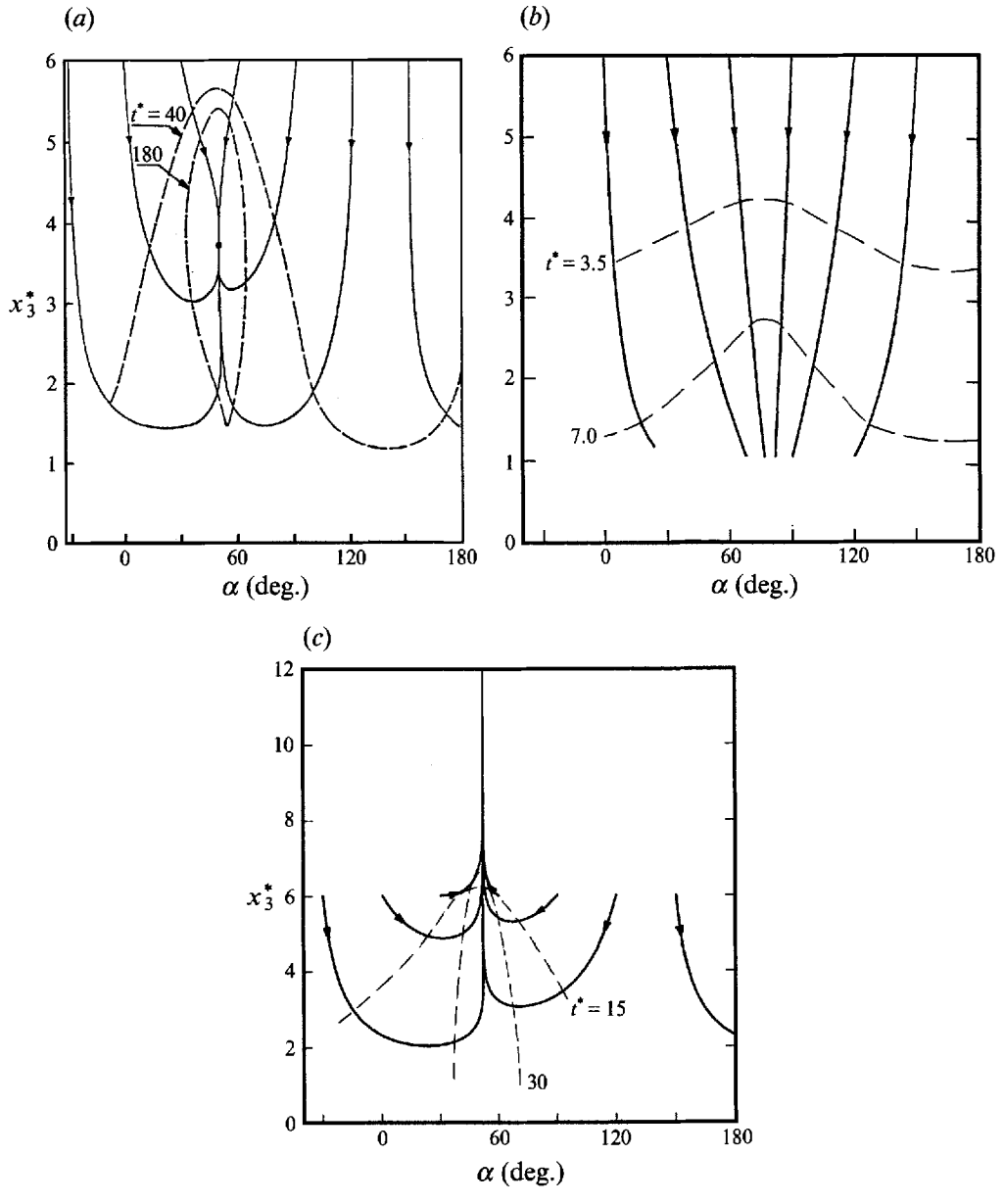

FIGURE 15. Trajectories of an oblate spheroid settling under gravity adjacent to an inclined plane from the initial position $x_3^* = 6$ in terms of the separation distance and the orientation angle relative to the wall. (*a*) $\epsilon = 0.5$, $\beta = 85°$; (*b*) $\epsilon = 0.1$, $\beta = 30°$; (*c*) $\epsilon = 0.1$, $\beta = 81°$; ——, trajectories; ---, constant elapsed time; ., equilibrium position. Dimensionless variables defined following (4.9).

in figure 15. Figure 15(*a*) shows that all the curves (solid lines) coalesce to the same point indicating that for a given particle geometry and wall inclination angle, both the final equilibrium separation distance and the particle orientation angle are independent of the initial position. In figure 15(*b*) the curves appear to be converging together although it is not clear whether they coalesce to the same point. The dashed lines in figure 15 represent the positions for which the particle would take the same amount of time to reach if it were released at $x_3^* = 6$ but with different initial orientations. When

(*a*) $\epsilon = 0.1$

Oblate spheroid			Prolate spheroid		
β (deg.)	x_3^*	α (deg.)	β (deg.)	x_3^*	α (deg.)
70	1.10	62.0	77	1.40	148.2
71	1.22	61.5	78	2.34	145.3
72	1.32	60.4	79	5.76	143.4
73	1.44	59.5	79.7	∞	142.7
74	1.62	58.6			
75	1.85	57.5			
76	2.16	56.5			
77	2.64	55.4			
78	3.46	54.4			
79	5.20	53.4			
80	12.2	52.5			
80.6	∞	51.9			

(*b*) $\epsilon = 0.5$

β (deg.)	x_3^*	α (deg.)	β (deg.)	x_3^*	α (deg.)
80	1.13	57.3	83	1.30	145.6
81	1.27	56.0	84	1.79	142.7
82	1.45	54.6	85	3.07	139.9
83	1.77	52.6	86	24.1	138.0
84	2.34	51.2	86.1	∞	137.9
85	3.70	49.5			
86	18.7	48.0			
86.2	∞	47.8			

TABLE 9. The separation distance x_3^* and particle orientation angle α at the equilibrium position for a spheroid settling under gravity adjacent to a plane inclined at angle β

the particle has reached the equilibrium position it translates parallel to the wall without rotation at a constant velocity. In this position, the gravitational component perpendicular to the wall is exactly balanced by the lift force due to the parallel motion and simultaneously the torque due to the parallel motion is exactly balanced by the torque from the pressure distribution on the surface as explained earlier. If the particle is slightly displaced perpendicular to the wall from the equilibrium position, a restoring force acts to return it to the equilibrium position. Moreover, if the equilibrium orientation of the particle is slightly disturbed, a restoring torque acts to return the particle to its equilibrium orientation. Thus the particle is in stable equilibrium. The equilibrium position depends on the aspect ratio of the particle and the inclination angle of the wall. If the inclination angle of the wall β is decreased, the component of gravity perpendicular to the wall increases and thus the equilibrium position moves closer to the wall where the lift force is greater. Table 9 shows the final separation distance and orientation angle for selected inclination angles β for an oblate or prolate spheroid having aspect ratios $\epsilon = 0.1$ and 0.5. As the inclination angle approaches the asymptotic value denoted by β_∞, the equilibrium separation distance x_3^* becomes infinite. The asymptotic values of α and β shown as the last entry on table 9 were obtained from analytic expressions derived in Appendix A using the weak interaction theory of Wakiya (1959). No equilibrium solutions exist for $\beta_\infty < \beta \leqslant 90°$. In this range of β, the particle rotates and asymptotically approaches α_∞ as shown in figure 15(*c*). The particle may move initially toward or away from the wall depending on the

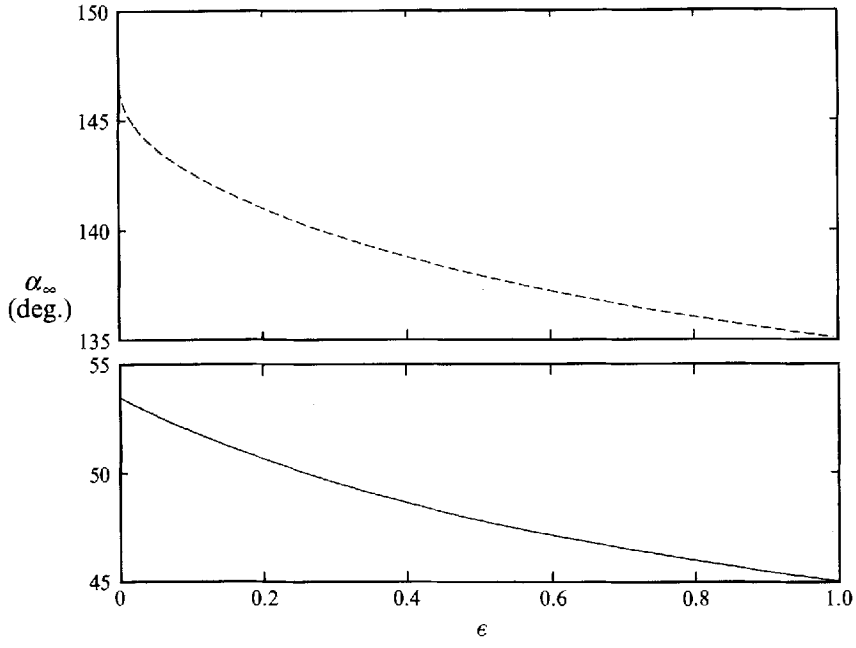

FIGURE 16. Asymptotic equilibrium orientation angle; ——, oblate spheroid; – – –, prolate spheroid.

initial orientation angle α_0 (see figure 14*c*). After reaching α_∞, the particle drifts away from the wall without rotation.

5. Concluding remarks

In this paper, the velocities and trajectories of a neutrally buoyant spheroidal particle in shear flow in the vicinity of a planar wall and a non-neutrally buoyant spheroidal particle settling under gravity adjacent to an inclined plane have been computed utilizing the solutions of the resistance tensor obtained by Hsu & Ganatos (1989) using the boundary integral method. The method has been successful in producing highly accurate solutions down to particle–wall gap widths of $0.1c$ with modest computational resources.

In closing, the authors wish to mention two extensions of the present theory currently in progress at The City College of New York. One extension involves an arbitrary particle in the vicinity of a planar boundary with a circular hole. The other involves an arbitrary particle in a parallel walled channel.

This research was supported by a Research Initiation Grant from the National Science Foundation, no. CME81-05914 and by a grant from The City University of New York PSC-CUNY Research Award Program, no. 663310. Their support is gratefully acknowledged. The authors also wish to thank The City University of New York Computer Center and The City College of New York Computer Center for the use of their facilities.

Appendix A

In this Appendix, asymptotic expressions are presented for the equilibrium particle orientation angle and wall inclination angle for a spheroidal particle settling under gravity adjacent to an inclined plane. The expressions are based on the method of reflections theory of Wakiya (1959).

At the equilibrium position, the particle translates parallel to the wall without rotation and maintains a constant distance from the wall. Setting $U_3 = \omega = 0$ in (4.1) yields

$$6\pi\mu c F_1^{t_1} U_1 + \tfrac{4}{3}\pi ab^2(\rho_s - \rho) g \sin\beta = 0, \tag{A 1a}$$

$$6\pi\mu c F_3^{t_1} U_1 - \tfrac{4}{3}\pi ab^2(\rho_s - \rho) g \cos\beta = 0, \tag{A 1b}$$

$$T_2^{t_1} U_1 = 0. \tag{A 1c}$$

Dividing (A 1*a*) by (A 1*b*) gives

$$\tan\beta = -\frac{F_1^{t_1}}{F_3^{t_1}}, \tag{A 2}$$

and (A 1*c*) requires

$$T_2^{t_1} = 0. \tag{A 3}$$

At large particle–wall spacings, asymptotic expressions for the force and torque coefficients are presented by Wakiya (1959). The leading terms of these asymptotic expansions are

$$F_1^{t_1} = -\frac{8}{3c}\left[\frac{\cos^2\alpha}{K + a^2 L_1} + \frac{\sin^2\alpha}{K + b^2 L_3}\right]\left[1 + \frac{3}{2H}\left(\frac{1+\sin^2\alpha}{K + a^2 L_1} + \frac{1+\cos^2\alpha}{K + b^2 L_3} - \frac{2}{K + a^2 L_1 \sin^2\alpha + b^2 L_3 \cos^2\alpha}\right)\right], \tag{A 4}$$

$$F_3^{t_1} = \frac{8}{3c}\left[\frac{1}{K + a^2 L_1} - \frac{1}{K + b^2 L_3}\right]\left[1 + \frac{3}{2H}\left(\frac{1+\sin^2\alpha}{K + a^2 L_1} + \frac{1+\cos^2\alpha}{K + b^2 L_3}\right)\right]\sin\alpha\cos\alpha, \tag{A 5}$$

$$T_2^{t_1} = -\frac{3(a^2 - b^2)}{16bH^2(a^2 L_1 + b^2 L_3)}[F_1^{t_1}\cos 2\alpha - \tfrac{3}{2}F_3^{t_1}\sin 2\alpha], \tag{A 6}$$

where

$$K = \int_0^\infty \frac{\mathrm{d}s}{\Delta}, \quad L_1 = \int_0^\infty \frac{\mathrm{d}s}{(a^2+s)\Delta}, \quad L_3 = \int_0^\infty \frac{\mathrm{d}s}{(b^2+s)\Delta}, \tag{A 7a–c}$$

and

$$\Delta = (a^2+s)^{\frac{1}{2}}(b^2+s). \tag{A 8}$$

Substitution of (A 6) into (A 3) yields

$$\tan 2\alpha_\infty = \frac{2F_1^{t_1}}{3F_3^{t_1}}. \tag{A 9}$$

Elimination of the force coefficients between (A 2) and (A 9) provides a simple relationship between the asymptotic equilibrium particle orientation angle and the wall inclination angle

$$\tan\beta_\infty = -\tfrac{3}{2}\tan 2\alpha_\infty. \tag{A 10}$$

Finally, substituting (A 4) and (A 5) into (A 9) and dropping terms $O(1/H)$ leads to an explicit expression for the asymptotic equilibrium orientation angle solely in terms of particle aspect ratio ϵ:

$$\cos 2\alpha_\infty = -A \pm (A^2+3)^{\frac{1}{2}}, \tag{A 11}$$

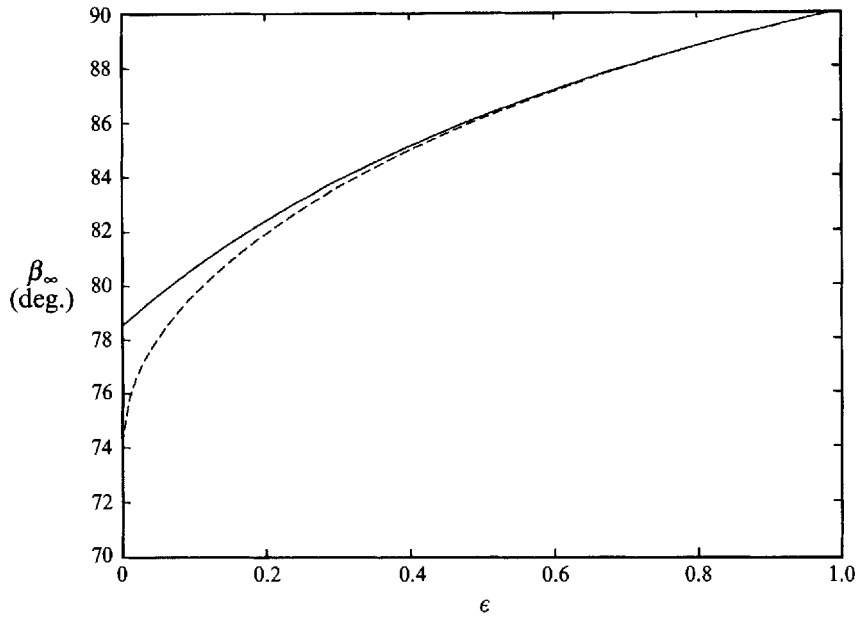

FIGURE 17. Asymptotic equilibrium wall inclination angle; ——, oblate spheroid; – – –, prolate spheroid.

where
$$A = \frac{2K + a^2 L_1 + b^2 L_3}{a^2 L_1 - b^2 L_3}. \tag{A 12}$$

In (A 11) the positive sign is used for a prolate spheroid and the negative sign is used for an oblate spheroid.

Figure 16 shows a plot of the asymptotic equilibrium orientation angle α_∞ as a function of particle aspect ratio ϵ. The corresponding asymptotic equilibrium wall inclination angles are shown in figure 17. In both figures, the solid curve is for an oblate spheroid and the dashed curve is for a prolate spheroid. For an oblate spheroid located far from the wall having an aspect ratio of zero (i.e. a flat disk) the equilibrium wall inclination angle is 78.5° with a corresponding particle orientation angle of 53.5°. As the particle aspect ratio is increased to unity (i.e. as the particle becomes spherical), the equilibrium wall inclination angle approaches 90° and the particle orientation angle approaches 45°. Of course, the particle orientation angle has no significance for a spherical particle. For a prolate spheroid located far from the wall with an aspect ratio of zero (i.e. a rod-like object), the equilibrium wall inclination angle is 70.7° with a corresponding particle orientation angle of 148.8°. As the aspect ratio is increased to unity, the equilibrium wall inclination angle approaches 90° and the particle orientation angle approaches 135°.

As shown in table 9, at closer particle–wall spacings, all equilibrium solutions lie above the two limiting curves in figure 16 and below the two limiting curves in figure 17. Thus for a given particle aspect ratio, there is a range of wall inclination angles, $\beta_\infty < \beta \leqslant 90°$, where the wall is nearly vertical and no equilibrium solutions exist.

REFERENCES

BLAKE, J. R. 1971 A note on the image system for a stokeslet in a no-slip boundary. *Proc. Camb. Phil. Soc.* **70**, 303.

BRENNER, H. 1961 The slow motion of a sphere through a viscous fluid towards a plane surface. *Chem. Engng Sci.* **16**, 242.

BRENNER, H. 1964 The Stokes resistance of an arbitrary particle – II. An extension. *Chem. Engng Sci.* **19**, 599.

DABROS, T. 1985 A singularity method for calculating hydrodynamic forces and particle velocities in low-Reynolds-number flows. *J. Fluid Mech.* **156**, 1.

GOLDMAN, A. J., COX, R. G. & BRENNER, H. 1967*a* Slow viscous motion of a sphere parallel to a plane wall. I. Motion through a quiescent fluid. *Chem. Engng Sci.* **22**, 637.

GOLDMAN, A. J., COX, R. G. & BRENNER, H. 1967*b* Slow viscous motion of a sphere parallel to a plane wall. II. Couette flow. *Chem. Engng Sci.* **22**, 653.

HAPPEL, J. & BRENNER, H. 1973 *Low Reynolds Number Hydrodynamics*, 2nd rev. edn. Noordhoff.

HSU, R. & GANATOS, P. 1989 The motion of a rigid body in viscous fluid bounded by a plane wall. *J. Fluid Mech.* **207**, 29.

JEFFERY, G. B. 1922 The motion of ellipsoidal particles immersed in a viscous fluid. *Proc. R. Soc. Lond.* A **102**, 161.

WAKIYA, S. 1959 Effect of a submerged object on a slow viscous flow (Report V). Spheroid at an arbitrary angle of attack. *Res. Rep. Fac. Engng Niigata Univ. (Japan)* **8**, 17 (in Japanese).

YANG, S. M. & LEAL, L. G. 1983 Particle motion in Stokes flow near a plane fluid–fluid interface. Part 1. Slender body in a quiescent fluid. *J. Fluid Mech.* **136**, 393.

YANG, S. M. & LEAL, L. G. 1984 Particle motion in Stokes flow near a plane fluid–fluid interface. Part 2. Linear shear and axisymmetric straining flows. *J. Fluid Mech.* **149**, 275.